

UNAEN: Unsupervised Abnormality Extraction Network for MRI Motion Artifact Reduction

Yusheng Zhou, Hao Li, Jianan Liu, Zhengmin Kong, Tao Huang, *Senior Member, IEEE*,
Euijoon Ahn, and Zhihan Lv, *Senior Member, IEEE*

Abstract— Motion artifact reduction is one of the most concerned problems in magnetic resonance imaging. In recent years, deep learning-based methods have been widely investigated for artifact reduction tasks in MRI. As a retrospective processing method, neural network does not cost additional acquisition time or require new acquisition equipment, and seems to work better than traditional artifact reduction methods. In the previous study, training such models require the paired motion-corrupted and motion-free MR images. However, it is extremely tough or even impossible to obtain these images in reality because patients have difficulty in maintaining the same state during two image acquisition, which makes the training in a supervised manner impractical. In this paper, we proposed a new unsupervised abnormality extraction network (UNAEN) to alleviate this problem. Our network realizes the transition from artifact domain to motion-free domain by processing the abnormal information introduced by artifact in unpaired MR images. Different from directly generating artifact reduction results from motion-corrupted MR images, we adopted the strategy of abnormality extraction to indirectly correct the impact of artifact in MR images by learning the deep features. Experimental results show that our method is superior to state-of-the-art networks and can potentially be applied in real clinical settings.

Index Terms— Magnetic Resonance Imaging, Motion Artifact Reduction, Unsupervised Learning.

I. INTRODUCTION

MAGNETIC resonance imaging (MRI) is a non-invasive medical imaging technique used in the diagnosis of various diseases without radiation exposure. However, due to the long acquisition time, MRI is sensitive to the patient's movement [1], and incorrect K-space signal filling cause blurring or ghosting artifacts, which in turn affects the patient's

This work has been submitted to the IEEE for possible publication. Copyright may be transferred without notice, after which this version may no longer be accessible.

Yusheng Zhou and Hao Li contribute equally to the work and are co-first authors. (Corresponding Author: Zhengmin Kong)

Yusheng Zhou and Zhengmin Kong are with School of Electrical Engineering and Automation, Wuhan University, China. (Email: 2017301470075@whu.edu.cn; zmkong@whu.edu.cn)

Hao Li is with the Department of Neuroradiology, University Hospital Heidelberg, Heidelberg, Germany. (email: hao.li@med.uni-heidelberg.de)

Jianan Liu is with Vitalent Consulting, Gothenburg, Sweden. (Email: jianan.liu@vitalent.se)

Tao Huang and Euijoon Ahn are with the College of Science and Engineering, James Cook University, Cairns, Australia. (Email: tao.huang1@jcu.edu.au; euijoon.ahn@jcu.edu.au)

Zhihan Lv is with the Department of Game Design, Faculty of Arts, Uppsala University, Sweden (Email: lvzhihan@gmail.com)

diagnosis. To solve motion-related problems, researchers have proposed a variety of methods to prevent movement or correct artifacts [2]–[8]. An effective method is to introduce new equipment, such as MR navigators [9], [10] or external tracking devices [11], to accelerate the acquisition and compensate or reacquire the K-space data partially in a prospective manner. Although it can significantly prevent the generation of motion artifacts, it has not been widely applied due to the expensive additional cost. Another type of solutions to artifact correction are commonly based on traditional non-learning statistical signal processing retrospectively. For example, [7] used an entropy focus criterion to compensate for motion-induced artifacts in an MR image, [8] described that a general matrix equation gives the corrupted image from the ideal object and the ideal image can be got from the corrupted one by reversing this system, and so on. Retrospective techniques made use of priori motion information to explore the influence of motion on K-space data from the physical level and build models, where the motion-free image could be reconstructed. However, a fatal flaw of statistical analysis methods is the computational limits because of the diversity of artifacts.

In recent years, artifact reduction techniques which are based on supervision and deep learning, have been proposed to address the artifact problem in MRI [12]–[14]. It does not increase scanning time and requires no additional acquisition equipment. A large number of training samples are used to train neural networks. Motion-free MR images is used as the correction guide to reduce artifacts in paired motion-corrupted MR images, showing better performance over traditional non-learning methods in several studies. However, the acquisition of paired MR images is extremely tough or even impossible due to the difficulty in maintaining the same state of the patients during the two image acquisition. Image misalignment caused by state deviation is mistakenly considered as a type of artifact, and then descends the artifact reduction ability of the model, restricting the use of these method in real clinical practice.

It is necessary to develop training methods that are applicable when only no paired MR images are available [15], [16], and the successful popularization of unsupervised learning in various tasks in the field of computer vision [17]–[21] gives us a possible way to solve above problems. As another branch of deep learning, unsupervised learning can find hidden patterns or features from data without requiring feedback information such as labels or categories, and does not overly rely on prior knowledge of dataset. In particular, several recent

models based on unsupervised learning have shown promising results without paired training samples, such as ISCL [22] and UIDnet [23] for image denoising task, ADN [24] for computed tomography (CT) metal artifact reduction (MAR) task proposed by Liao *et al.* and CycleGAN [25] proposed by Zhu *et al.* for realizing images style transfer. **These tasks are similar to motion artifact reduction so that we can draw on empirical reference from them.**

As a common basis of the methods mentioned above, generative adversarial network (GAN) [17] is one of the most attractive technologies at present and one of the most promising methods to handle the distribution of complex data. Originally designed to generate data that doesn't exist in the real world, GAN comes in many variations for different tasks [25]–[29]. Especially in the field of image generation, including unconditional generation [17], [27], conditional generation [26], [28] and image-to-image translation [25], [29], etc., GAN's studies have accumulated a solid fundamental of knowledge. In order to avoid the unavailability of paired MR images, we proposed an unsupervised MRI artifact reduction framework inspired by GAN, which trains the network by using unpaired motion-free MR images and motion-corrupted MR images. The contributions of this work are summarized as follows:

- We proposed an unsupervised abnormality extraction network (UNAEN) to extract artifact residual maps by learning the deep feature differences between unpaired motion-free images and motion-corrupted images, indirectly achieving the reduction of motion artifacts in MR images.
- Different from the existing methods in the literature, UNAEN aimed to extract the abnormal information explicitly in the image that causes the deep features difference, and eliminated these abnormal information to make the motion-corrupted close to the motion-free distribution, improving the model's representation learning ability of artifact.
- Experimental results showed that compared with some unsupervised models, the proposed model got higher evaluation metrics and generated image with superior quality.

II. RELATED WORK

A. Conventional Artifact Reduction

The most straightforward method to address the problem of motion artifacts in MRI is to restrain the patients' motions by means of sedation or breath-holding during K-space data acquisition [2]. However, patients cannot control physiological involuntary movements such as cerebrospinal fluid pulsation or intestinal peristalsis. In order to reduce the burden on patients, some fast acquisition strategies have been proposed. Compressed sensing [3] is an acquisition and reconstruction technique based on signal sparsity, and its application to K-space undersampling can shorten the scan time. Parallel imaging [4] technique uses multiple coils with different sensitivities to collect data during MR scanning to reduce the phase encodings and thus the scan time. Although these methods to

accelerate the acquisition of K-space data can suppress motion artifacts to a certain extent, they do not fundamentally solve the problem.

Traditional artifact reduction methods include prospective methods and retrospective methods. Prospective motion artifact correction [5], [6] can compensate or reacquire K-space partially throughout the scan by measuring the patient motion repeatedly, which has great potential. But because of requiring additional expensive hardware, it has not been widely used in the clinic. Unlike the prospective methods, the retrospective methods lessen the concern of imperfect motion information corrupting the acquisition. Retrospective motion artifact correction [7], [8] have attempted to utilize the priori motion information to estimate artifact. But these algorithms are computationally limited due to the complexity and unpredictability of patients' motions. Overall, the traditional algorithms mentioned above all have some shortcomings when dealing with the motion artifacts.

B. Deep Artifact Reduction

With the great success of deep learning in the field of computer vision, some researchers have proposed retrospective artifact reduction schemes based on deep learning (especially convolutional neural network, CNN). The CNN model can be trained with motion-corrupted images as input and the same individual's motion-free images as ground truth. As one of the first studies for motion correction using deep learning, Johnson *et al.* reconstructed the motion-corrected MR image from the vector of motion-deformed k-space by the deep neural network (DNN) [13]. Han *et al.* proposed a denoising algorithm based on U-net to remove the streak artifacts induced in images obtained via radial acquisition [12]. And Sommer *et al.* applied a fully CNN to extracted motion artifact-only image, which subtracts the motion-clean image from the motion-corrupted image, resulting in less deformation [14]. However, in most cases it is difficult or impossible to obtain paired MRI dataset to train neural networks. Although several algorithms on motion simulation have been proposed to solve this problem, these algorithms only consider simple and fixed motion patterns to corrupt MR images from the image domain [30] or K-space [31], [32]. In fact, the motion of patients is more random and unpredictable. Models trained on datasets generated by simulation artifacts perform poorly in practical applications.

C. Unsupervised Image-to-Image Translation

Artifact reduction can be regarded as a task of image-to-image translation. In recent years, some training strategies based on unpaired images have attracted much attention. Deep Image Prior (DIP) [33] demonstrated the feasibility of hand-crafted prior generated by a randomly initialized network for image denoising task. However, the disadvantage is that a large amount of resources are consumed for iterative computation for each image. Noise2Noise (N2N) [34] and Noise2Void (N2V) [35] only used noisy images to train a CNN denoiser. Although satisfactory denoising effect can be achieved without noisy-clean image pairs, it is also necessary to know the

distribution of pixel-independent noise in order to choose the applicable loss functions. Recently, generative adversarial network (GAN) [17] had shown great potential in image generation and representation learning. The GCBD [36] proposed by Chen *et al.* illustrated that GAN can train to estimate the noise distribution of the noisy images. UIDnet [23] applied a conditional GAN (cGAN) [28] to generate clean-pseudo noisy pairs for training a denoising network. CycleGAN [25], [29] is a cyclic symmetric network consisted of two generators and two discriminators, which is mainly used for domain adaption. ISCL [22] added a noise extractor on the basis of CycleGAN for cooperative learning with the generators. By combining generative model and disentanglement network, ADN [24] constructed multiple encoders and decoders to separate the contents and artifacts in the CT images and get comparable results with supervised learning.

III. PROPOSED METHOD

In this work, an unsupervised de-motion artifact model named Unsupervised Abnormality Extraction Network (UNAEN) which uses the unpaired MR images to train, is proposed as shown in Fig.1. In order to promote the representation learning ability of motion artifact, an artifact extractor was designed to intercept the artifact residual maps from the motion-corrupted MR images, instead of using the generator to directly generate the motion correction result. Compared with general GAN, the mapping function between artifact domain and motion-free domain could be obtained more easily. In addition, we used an artifact reconstructor to restore the original input from the motion artifact-reduced images to prevent the artifact extractor from mismapping. In the experiment, we compared the performance of UNAEN with some state-of-the-art models such as CycleGAN, ISCL, UIDnet. The experimental results show that our proposed model can achieve better artifact reduction effect.

A. Network Architecture

Specifically, the UNAEN framework contains two modules: forward module for artifact reduction and backward module for artifact reconstruction. The forward module comes with an artifact extractor G_e for learning the artifact distribution in the motion-corrupted MR images. There is an artifact reconstructor G_r in the backward module that restores the corresponding original input from the output generated by the forward module. We take the unpaired images $\{(x^a, y) | x^a \in X^a, y \in Y\}$ as training samples, where X^a and Y represent the motion-corrupted MRI set and motion-free MRI set, respectively. The G_e and G_r are both generators of UNAEN. To train generators, we employed D_f and D_b as discriminators in the forward and backward modules to distinguish between a real sample and a fake sample.

The workflow of UNAEN is shown as the arrows in the Fig.1. We took the motion-corrupted MR image x^a as input fed into G_e to extract the artifact residual map $G_e(x^a)$, which affects the texture information of MRI. The forward module will generate the corresponding artifact-reduced image x by

subtracting $G_e(x^a)$ from x^a :

$$x = x^a - G_e(x^a), \quad (1)$$

To enable the forward module to translate an instance x^a into a counterpart x rather than any instance, we introduced the backward module. The main target of G_r is to translate back the x into the original x^a . So G_r is used to restore the generated x and output the restored artifact-corrupted image \bar{x}^a :

$$\bar{x}^a = G_r(x), \quad (2)$$

There is a cycle consistency between x^a and \bar{x}^a and they are expected to be identical. Since x and y are unpaired and only have similar content, a forward discriminator D_f should be applied to distinguish between the generated image x and real motion-free image y . To promote the reconstruction ability of \bar{x}^a , we train a backward discriminator D_b to distinguish between the original input x^a and restored artifact-corrupted result \bar{x}^a .

During the training step, we train the generators and discriminators alternately. The generators aim to generate samples that are closed to real data while discriminators try not to be deceived by the output of generators. During the inference step, only the trained G_e are required. We can obtain the motion artifact-reduced images as long as we subtract the artifact residual maps extracted by the G_e from corresponding motion-corrupted inputs. More details about generators and discriminators will be discussed in the following subsection.

B. Loss Functions

In our experiments, we employed three types of loss functions which are the L1 loss, SSIM (Structural Similarity Index Measure) loss [37], [38] and adversarial loss:

$$L_1(x, y) = \frac{1}{N} \sum_{i=1}^N |x - y| \quad (3)$$

$$L_{SSIM}(x, y) = \frac{1}{N} \sum_{i=1}^N |1 - SSIM(x, y)^2| \quad (4)$$

$$L_{adv}(x, D) = \frac{1}{N} \sum_{i=1}^N \sqrt{(D(x) - 1)^2} \quad (5)$$

where D represents the D_f or D_b . SSIM (Structural Similarity Index Measure) is an indicator to quantify the similarity between two digital images. See Eq.(10) for specific formula. In addition, we use the least square loss [39] as the adversarial loss in our model instead of the negative log likelihood [17] for stabilizing the training procedure.

To train G_e , we use a discriminator D_f which aims to classify the motion artifact-reduced output x as a motion-free image. The adversarial loss function L_{G_e} as follow:

$$L_{G_e,adv}(x, D_f) = \frac{1}{N} \sum_{i=1}^N \sqrt{(D_f(x) - 1)^2} \quad (6)$$

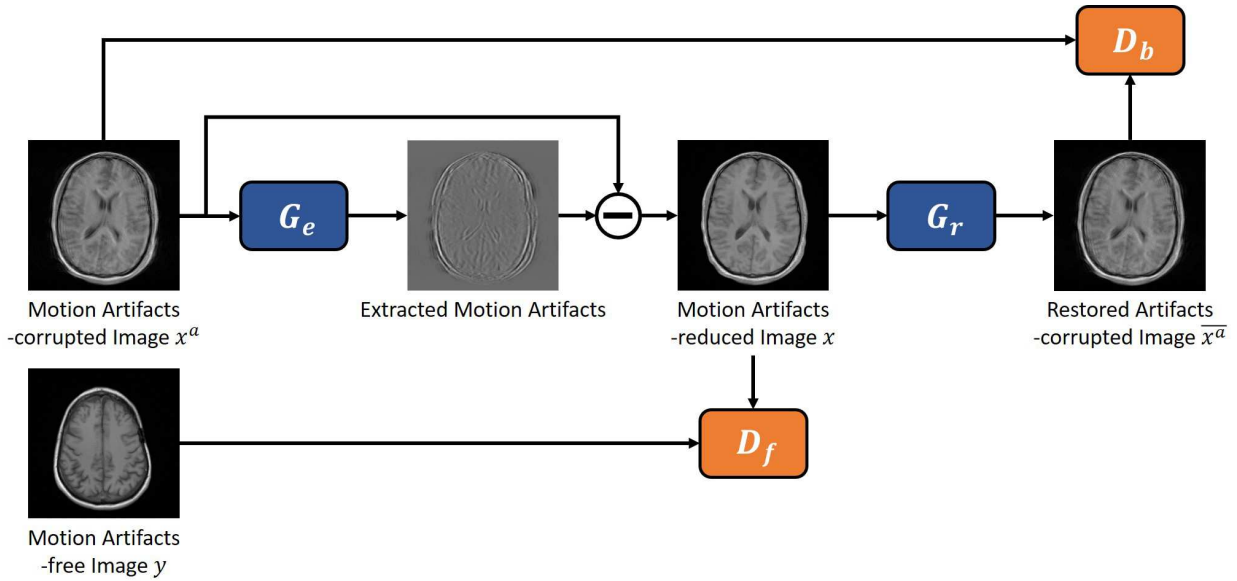


Fig. 1. The architecture of UNAEN. It consists of two generators and two discriminators. The network is fed unpaired motion artifact-corrupted and motion artifact-free images in training. Motion artifact reduced output can be obtained by subtracting the artifact residual map extracted by G_e from motion-corrupted input, and G_r converts the output to original input. D_f compared the output with motion artifact-free input to identify whether the artifact removal is successful while D_b is used to check whether G_r is restored successfully.

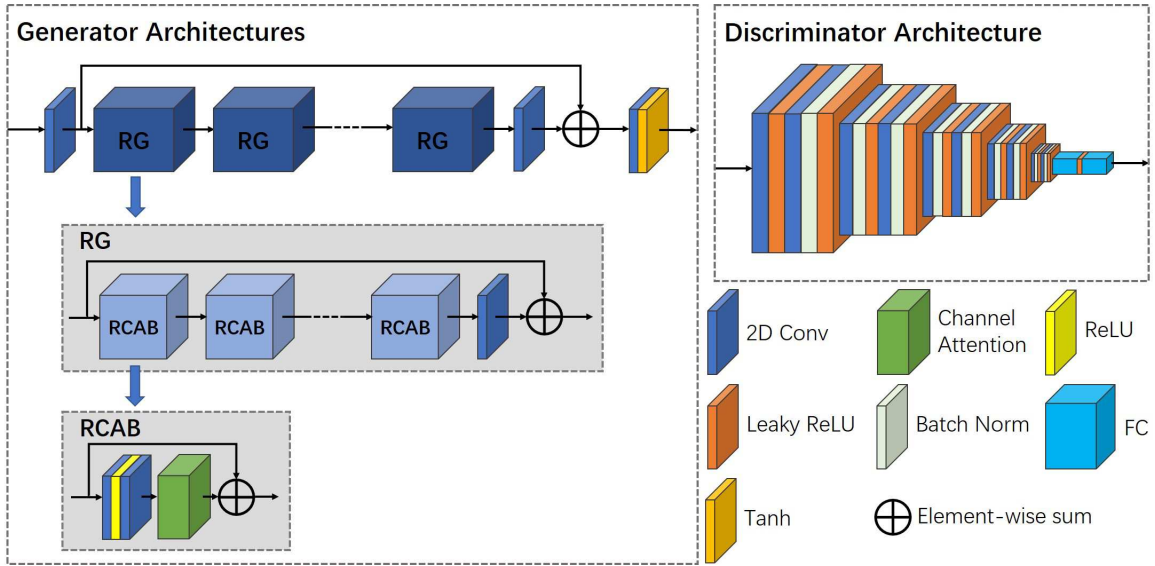


Fig. 2. The detailed structures of generator and discriminator. The generator adopt the RCAN backbone with a depth of 5 residual groups (RG) and a long skip connection, and the discriminator is a VGG network.

To train G_r , we use a discriminator D_b which aims to classify the restored artifact-corrupted result \bar{x}^a as the original motion-corrupted image. The following adversarial loss function is used to train the G_r :

$$L_{G_r\text{-}adv}(\bar{x}^a, D_b) = \frac{1}{N} \sum_{i=1}^N \sqrt{(D_b(\bar{x}^a) - 1)^2} \quad (7)$$

Moreover, we adopt the cycle consistency loss to restrain the restoration of \bar{x}^a . It is calculated as a weighted sum of L1 loss and SSIM loss between the input and reconstruction images:

$$L_{G_r\text{-}cyc}(x^a, \bar{x}^a) = L_1(x^a, \bar{x}^a) + \lambda_{SSIM} * L_{SSIM}(x^a, \bar{x}^a) \quad (8)$$

where λ_{SSIM} is the weight of SSIM loss. We set $\lambda_{SSIM} = 0.5$ in our experiments.

So, the final objective function that optimizes the G_e and G_r networks can be represented as:

$$L_G = \lambda_{G_e\text{-}adv} * L_{G_e\text{-}adv} + \lambda_{G_r\text{-}adv} * L_{G_r\text{-}adv} + L_{G_r\text{-}cyc} \quad (9)$$

where $\lambda_{G_e\text{-}adv}$ and $\lambda_{G_r\text{-}adv}$ are the weights of the adversarial losses of G_e and G_r , respectively. We set $\lambda_{G_e\text{-}adv} = 0.1$ and $\lambda_{G_r\text{-}adv} = 0.1$ in our experiments.

C. Motion Simulation

We referred to the paper [40] to simulate the motion in MR images. The method of splicing lines from multiple K-space

was used to simulate the generation of real motion artifacts. Firstly, a group of images was generated from the original images by rotating them in specific directions and to specific degrees. The severity can be managed by the frequency of motion. Then the original image and the generated images were transformed to K-space using FFT, and K-space segments of the original image were replaced with segments from the generated images' K-spaces, according to a predefined pattern. Finally, the damaged original K-space data is transferred back to the image domain by iFFT to obtain the simulation motion-corrupted MR image.

In the process of motion simulation, we used the echo group (EG) as the minimum time period unit to obtain a certain number of successive echoes, and the duration of any action must be an integer multiple of EG. To simulate the motion of patients' head, we set the original images to be rotated 5 degrees to the left and to the right in plane. Specifically, we used the K-space segments of the rotated images to periodically replace the K-space segments of the original image from the center line to the edge line.

IV. EXPERIMENTS

In this section, a brief description of the dataset is presented, and implementation details, including the network architecture and hyper-parameters, are introduced. Experimental results are presented with analyses and discussions.

A. Dataset Description

In this study, the fastMRI brain dataset [41] is used to evaluate the proposed method. It includes 6970 fully sampled brain MRIs (3001 at 1.5T and 3969 at 3T) collected at NYU Langone Health on Siemens scanners using T1-weighted, T2-weighted, and FLAIR acquisitions. Some of the T1-weighted acquisitions included admissions of contrast agents. The Brain MRI DICOM set, which exhibits a wide variety of reconstruction matrix sizes, were acquired with a larger diversity of scanners, manners of acquisition, reconstruction methods, and post-processing algorithms. See paper [41], [42] for more details. To reduce the influence of external factors and MRI acquisition methods on the experiment results, we randomly selected 5000 slices only from the T1 weighted slices with 3T field strength, whose matrix size are 320 x 320.

In our experiments, the slices with large background in MR images were firstly discarded. All selected images were corrupted from the K-space by using a certain motion simulation algorithm mentioned above. Specifically, 1 EG contained 10 echos and the movement interval T_S was set to 3EG, 6EG and 9EG, resulting in a K-space corrupted line ratio of 75%, 60% and 50%, respectively. Then the dataset was divided into training set, validation set and test set. The unsupervised MRI de-motion artifact method requires unpaired motion-free MR images and motion-corrupted MR images, so we further divided the training set into two non-overlapping groups. One group contains only motion-free images as learning target while the other group contains only motion-corrupted images as input to the model. The validation set were used to monitor

the networks' performance during training and test set to evaluate the networks after training. All of images were normalized to 0 to 1. To save computation resource, we cropped images into 128 x 128 patches.

B. Evaluation Metrics

In order to make a comprehensive comparison, we used SSIM and PSNR as the basic evaluation metrics in our experiments.

As mentioned in III-B, SSIM can quantify the similarity of two images. It was defined to compare the brightness, contrast, and structure between the motion artifact-reduced output x and the ground truth. The SSIM is never greater than 1 and a larger value represents a better motion correction result. The specific expression is as follow:

$$SSIM(X, Y) = \frac{(2\mu_X\mu_Y + C_1)(2\sigma_{XY} + C_2)}{(\mu_X^2 + \mu_Y^2 + C_1)(\sigma_X^2 + \sigma_Y^2 + C_2)} \quad (10)$$

where μ and σ denote the mean and standard deviation of the images, respectively (σ_{XY}^2 donates the covariance of x and y). C_1 and C_2 are constants.

The PSNR (Peak Signal-to-Noise Ratio) is one of the widely employed image quality indicators, which represents the ratio between the maximum possible signal value and the interference noise value that affects the signal representation accuracy. It is usually measured in decibels (db) and a higher value indicates a lower distortion. PSNR can be calculated according to the following formula:

$$PSNR = 10 \log_{10} \frac{MaxValue^2}{MSE} \quad (11)$$

$$MSE = \frac{1}{mn} \sum_{i=0}^{m-1} \sum_{j=0}^{n-1} [I(i, j) - K(i, j)]^2 \quad (12)$$

where $MaxValue$ is the largest possible pixel value and MSE calculates the mean square error of two images. It is difficult for human eyes to perceive the difference when PSNR exceeds 30.

C. Experiment Configurations

We constructed two generators (artifact extractor G_e and artifact reconstructor G_r) and two discriminators to train UNAEN. The detailed structure of all networks as shown in the Fig.2. The backbone of generator was built by the Residual Channel Attention Network (RCAN) [43], [44] with a depth of 5 residual groups (RG) and a long skip connection. Each residual group (RG) has 5 residual channel attention blocks (RCAB) and a long skip connection. We set the number of feature channels to 64 at each base block of the generator. For the discriminator, we just used simple convolutional units to build the network, each unit consists of a 3 x 3 convolutional layer and a leaky rectified linear unit (leaky ReLU) activation layer [45]. The size of feature map was reduced by half after each two convolution. All but the first unit have a batch normalization layer [46]. Similarly, we set the number of feature channels to 64 in the first convolutional layer of the discriminator and doubled after each two convolutional layer.

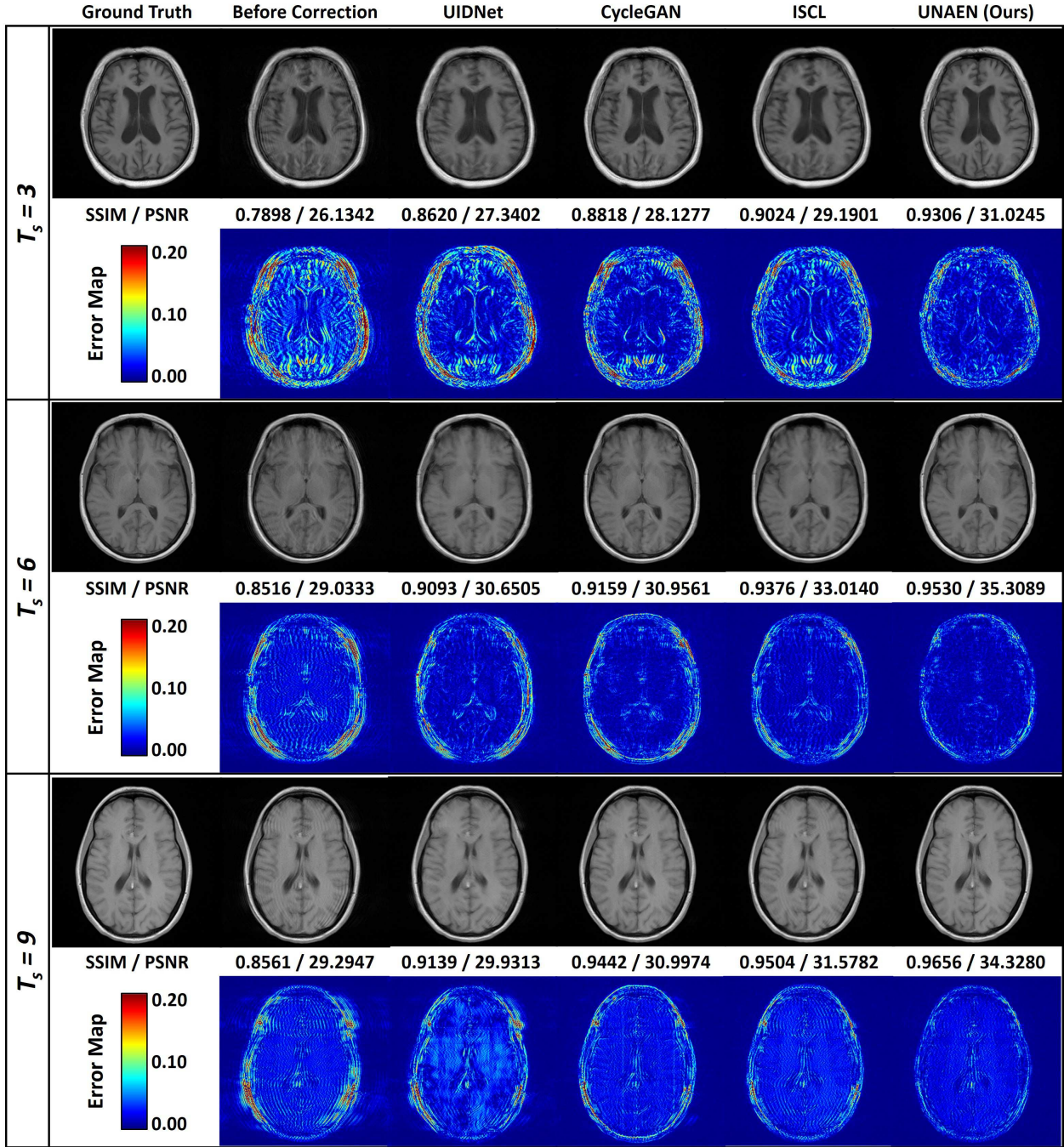


Fig. 3. Comparison of the qualitative performance of UNAEN and other unsupervised models on the fastMRI brain dataset. There visualized the artifact reduction results with varying degrees of artifact severity and corresponding error heat maps showing the difference between ground truth and each result.

All of our experiments were implemented on a desktop system with 64GB RAM and two NVIDIA GeForce RTX 2080 Ti graphics cards and used torch 1.8.1 as the back end. Before each epoch of training process, all the motion-free and motion-corrupted image patches were shuffled. We trained our model for 50 epochs using the ADAM optimizer with $\beta_1 = 0.9$, $\beta_2 = 0.99$ and set batch size to 4. In each batch, the motion-free patches and motion-corrupted patches fed to the networks were unpaired. The initial learning rate was set to 10-4 and dropped by half every 10 epochs. The generators were trained twice

for every time the discriminators trained.

D. Artifact Reduction on fastMRI

As shown in the top half of Table I, we compared the performance of the proposed model with other baseline methods on fastMRI brain datasets with varying degrees of artifacts severity. The SSIMs and PSNRs of the motion artifact-corrupted images revealed the severity difference of motion artifacts. We observed that the proposed unsupervised model was significantly superior to all comparison unsupervised

TABLE I

QUANTITATIVE COMPARISON WITH THE STATE-OF-THE-ART UNSUPERVISED NETWORKS FOR MRI MOTION ARTIFACT REDUCTION

Dataset	Methods	$T_S=3\text{EG}$		$T_S=6\text{EG}$		$T_S=9\text{EG}$	
		SSIM	PSNR	SSIM	PSNR	SSIM	PSNR
fastMRI	Before Reduction	0.7981	26.6165	0.8824	30.4109	0.9225	33.4192
	UIDnet (AAAI 2020) [23]	0.8551	27.1392	0.9168	30.4248	0.9411	32.5677
	CycleGAN (ICCV 2017) [25], [29]	0.8714	27.4449	0.9261	31.1473	0.9559	33.4017
	ISCL (IEEE TMI 2021) [22]	0.8958	29.3085	0.9410	32.4944	0.9585	34.4717
	UNAEN (Ours)	0.9126	30.5387	0.9504	33.5448	0.9674	35.9265

methods, where the SSIM was higher than 0.0089 to 0.0575 and the PSNR was higher than 1.0504 to 3.3995 dB according to experimental results.

Fig.3 visualized the artifact reduction effects of different model and showed the qualitative performance on three degrees of artifact severity by displaying the reduction results and corresponding error heat maps comparing to ground truth. All four unsupervised methods we compared (UIDnet, CycleGAN, ISCL, and UNAEN) successfully reduced the motion artifact. UIDnet seemed to have the weakest reduction ability and its outputs still retained significant artifact traces in the marginal region of the tissue. Similarly, CycleGAN generated blurry images even though it had a higher SSIM and PSNR than UIDnet. ISCL had better artifact reduction performance and improved image quality. However, evident errors on the boundaries of distinct soft tissues were observed in the reduction results, as shown in the error heat maps. On the contrary, UNAEN achieved higher metrics values and minimized errors, and with the increase of artifact severity, the performance gap with other methods was larger. In summary, UNAEN outperformed other compared models in terms of overall image quality and feature details in the experiment of fastMRI brain dataset.

V. DISCUSSION AND CONCLUSION

In this paper, we proposed an improved GAN model to get an artifact reduction network, which trained by unpaired MR images in an unsupervised manner to circumvent the difficulty of obtaining paired MR images. We conducted several experiments on two different dataset to qualitatively and quantitatively prove the outstanding performance of proposed model by compared to UIDnet, CycleGAN and ISCL.

Unlike other unsupervised networks, UIDnet trains a cGAN [28] which adds artifacts to clean images in order to generate paired images to train a de-artifacts network under supervision. Due to its indirect training strategy, more errors will be caused than other models, limiting the ability to remove artifacts and resulting in the fewest SSIM and PSNR in the experiments. The network error which represented as geometric uncertainty in image detail, could result in inaccurate surgery or therapy doses, indicating that the approach is less applicable in real clinics.

As an unsupervised network for domain transfer tasks, CycleGAN can transfer images between different styles. To generate a tighter mapping space, two symmetric generators are used to realize the conversion between motion-corrupted and motion-free image domains. The special learning method slightly promotes the artifact reduction effect while causes

the problem of calculation redundancy. However, most of the time we just need the artifact removal function rather than the reverse process, which would make training the model more difficult and cost more time. Consuming more computing resources is not proportional to the improvement in evaluation metrics.

ISCL is a variation of CycleGAN that adds an additional extractor and collaborates with generators for cooperative learning. The generators are responsible for direct conversion between image domains, while the extractor can extract artifacts from artifact observations. The experimental results showed that cooperative learning can further improve the SSIM and PSNR values at the cost of image blurring, which is actually not good for the visual effect and the help of doctors in diagnosis. Different from the CycleGAN and ISCL, UNAEN only adopted one cycle consistency and was more stable in training than CycleGAN and generated clearer results than ISCL. The abandonment of redundant training makes the model pay more attention to the artifact removal process and promote the representation ability of artifacts. Experimental results demonstrated that our modifications could successfully extract the artifact residual components of the images and suppress the motion artifact with little impact on the image quality, which significantly improved the metrics values and generated high quality artifact reduction results.

Given the effectiveness of UNAEN for unpaired images, we expect more applications to artifact reduction since obtaining paired images is commonly impractical. In the real clinical settings, UNAEN, as a retrospective method, can correct movements of patients to avoid the destruction of textures caused by artifacts. It is critical when researchers or medical staffs do not have access to the original data and associated reconstruction algorithms. In addition, we did not make assumptions about the nature of artifacts during the construction of UNAEN architecture, which makes it possible for the proposed model to be generalized in other artifact reduction problems, such as deblurring and denoising. We will further explore the possibility of realizing these extensions.

Despite the superior artifact reduction effect of UNAEN, there are still limitations in this study. Firstly, we generated artifacts of brain MRI only through simple periodic motion, but the movement of patients during K-space data acquisition may be more complex and irregular in real scenes. The performance of the proposed model trained with authentic motion-corrupted and motion-free images remains to be investigated. Besides, another limitation is that training the network is difficult, e.g., finding optimal hyper-parameters, due to complex loss

functions and adversarial networks. For the selection of some hyper-parameters, we directly gave the conclusions without listing relevant comparative experimental results, because their adjustments have limited impact on the overall performance of the network. We payed more attention to the modification of the model architecture, and the optimization of the details is one of goals of our future work.

REFERENCES

- [1] M. Zaitsev, J. Maclare, and M. Herbst, "Motion artifacts in mri: A complex problem with many partial solutions," *Journal of magnetic resonance imaging : JMRI*, vol. 42, no. 4, pp. 887–901, October 2015.
- [2] A. Stadler, W. Schima, A. Ba'ssalalah, J. Kettenbach, and E. Eisenhuber, "Artifacts in body mr imaging: Their appearance and how to eliminate them," *European radiology*, vol. 17, pp. 1242–55, 06 2007.
- [3] Z. Yang, C. Zhang, and L. Xie, "Sparse mri for motion correction," in *2013 IEEE 10th International Symposium on Biomedical Imaging*, 2013.
- [4] P. Noël, R. Bammer, C. Reinhold, and M. A. Haider, "Parallel imaging artifacts in body magnetic resonance imaging," *Canadian Association of Radiologists Journal*, vol. 60, no. 2, pp. 91–98, 2009.
- [5] N. White, C. Roddey, A. Shankaranarayanan, E. Han, D. Rettmann, J. Santos, J. Kuperman, and A. Dale, "Promo: Real-time prospective motion correction in mri using image-based tracking," *Magnetic Resonance in Medicine*, vol. 63, no. 1, pp. 91–105, 2010.
- [6] M. B. Ooi, S. Krueger, W. J. Thomas, S. V. Swaminathan, and T. R. Brown, "Prospective real-time correction for arbitrary head motion using active markers," *Magnetic Resonance in Medicine*, vol. 62, no. 4, pp. 943–954, 2009.
- [7] D. Atkinson, D. Hill, P. Stoyle, P. Summers, and S. Keevil, "Automatic correction of motion artifacts in magnetic resonance images using an entropy focus criterion," *IEEE Transactions on Medical Imaging*, vol. 16, no. 6, pp. 903–910, 1997.
- [8] P. Batchelor, D. Atkinson, P. Irarrazaval, D. Hill, J. Hajnal, and D. Larkman, "Matrix description of general motion correction applied to multi-shot images," *Magnetic Resonance in Medicine: An Official Journal of the International Society for Magnetic Resonance in Medicine*, vol. 54, no. 5, pp. 1273–1280, 2005.
- [9] Z. W. Fu, Y. Wang, R. C. Grimm, P. J. Rossman, J. P. Felmlee, S. J. Riederer, and R. L. Ehman, "Orbital navigator echoes for motion measurements in magnetic resonance imaging," *Magnetic resonance in medicine*, vol. 34, no. 5, pp. 746–753, 1995.
- [10] K. P. McGee, J. P. Felmlee, A. Manduca, S. J. Riederer, and R. L. Ehman, "Rapid autocorrection using prescan navigator echoes," *Magnetic Resonance in Medicine: An Official Journal of the International Society for Magnetic Resonance in Medicine*, vol. 43, no. 4, pp. 583–588, 2000.
- [11] J. Maclare, B. S. Armstrong, R. T. Barrows, K. Danishad, T. Ernst, C. L. Foster, K. Gumus, M. Herbst, I. Y. Kadashevich, T. P. Kusik *et al.*, "Measurement and correction of microscopic head motion during magnetic resonance imaging of the brain," *PloS one*, vol. 7, no. 11, p. e48088, 2012.
- [12] Y. Han, J. Yoo, H. H. Kim, H. J. Shin, K. Sung, and J. C. Ye, "Deep learning with domain adaptation for accelerated projection-reconstruction mr," *Magnetic resonance in medicine*, vol. 80, no. 3, pp. 1189–1205, 2018.
- [13] P. M. Johnson and M. Drangova, "Motion correction in mri using deep learning," in *Proceedings of the ISMRM Scientific Meeting & Exhibition, Paris*, vol. 4098, 2018, pp. 1–4.
- [14] K. Sommer, T. Brosch, R. Wiemker, T. Harder, A. Saalbach, C. S. Hall, and J. B. Andre, "Correction of motion artifacts using a multi-resolution fully convolutional neural network," in *Proceedings of the 26th Annual Meeting of ISMRM, Paris, France Abstract*, vol. 1175, 2018.
- [15] S. Laguna, R. Schleicher, B. Billot, P. Schaefer, B. McKaig, J. N. Goldstein, K. N. Sheth, M. S. Rosen, W. T. Kimberly, and J. E. Iglesias, "Super-resolution of portable low-field mri in real scenarios: integration with denoising and domain adaptation," in *Medical Imaging with Deep Learning*, 2022.
- [16] J. Liu, H. Li, T. Huang, E. Ahn, K. Han, A. Razi, and W. Xiang, "Unsupervised Representation Learning for 3D MRI Super Resolution with Degradation Adaptation," *arXiv e-prints*, p. arXiv:2205.06891, Nov. 2022.
- [17] I. Goodfellow, J. Pouget-Abadie, M. Mirza, B. Xu, D. Warde-Farley, S. Ozair, A. Courville, and Y. Bengio, "Generative adversarial networks," *Communications of the ACM*, vol. 63, no. 11, pp. 139–144, 2020.
- [18] J. Ho, A. Jain, and P. Abbeel, "Denoising diffusion probabilistic models," *Advances in Neural Information Processing Systems*, vol. 33, pp. 6840–6851, 2020.
- [19] D. P. Kingma and M. Welling, "Auto-Encoding Variational Bayes," *arXiv e-prints*, p. arXiv:1312.6114, Dec. 2013.
- [20] A. Van den Oord, N. Kalchbrenner, L. Espeholt, O. Vinyals, A. Graves *et al.*, "Conditional image generation with pixelcnn decoders," *Advances in neural information processing systems*, vol. 29, 2016.
- [21] L. Dinh, D. Krueger, and Y. Bengio, "NICE: Non-linear Independent Components Estimation," *arXiv e-prints*, p. arXiv:1410.8516, Oct. 2014.
- [22] K. Lee and W.-K. Jeong, "Iscl: Interdependent self-cooperative learning for unpaired image denoising," *IEEE Transactions on Medical Imaging*, vol. 40, no. 11, pp. 3238–3248, 2021.
- [23] Z. Hong, F. Xiaochen, T. Jiang, and J. Feng, "End-to-end unpaired image denoising with conditional adversarial networks," *Proceedings of the AAAI Conference on Artificial Intelligence*, vol. 34, pp. 4140–4149, 04 2020.
- [24] H. Liao, W.-A. Lin, S. K. Zhou, and J. Luo, "Adn: Artifact disentanglement network for unsupervised metal artifact reduction," *IEEE Transactions on Medical Imaging*, vol. 39, no. 3, pp. 634–643, 2020.
- [25] J.-Y. Zhu, T. Park, P. Isola, and A. A. Efros, "Unpaired image-to-image translation using cycle-consistent adversarial networks," in *Proceedings of the IEEE international conference on computer vision*, 2017, pp. 2223–2232.
- [26] T. Karras, S. Laine, and T. Aila, "A style-based generator architecture for generative adversarial networks," in *Proceedings of the IEEE/CVF conference on computer vision and pattern recognition*, 2019, pp. 4401–4410.
- [27] A. Radford, L. Metz, and S. Chintala, "Unsupervised Representation Learning with Deep Convolutional Generative Adversarial Networks," *arXiv e-prints*, p. arXiv:1511.06434, Nov. 2015.
- [28] M. Mirza and S. Osindero, "Conditional Generative Adversarial Nets," *arXiv e-prints*, p. arXiv:1411.1784, Nov. 2014.
- [29] K. Armanious, A. Tanwar, S. Abdulatif, T. Küstner, S. Gatidis, and B. Yang, "Unsupervised adversarial correction of rigid mr motion artifacts," in *2020 IEEE 17th International Symposium on Biomedical Imaging (ISBI)*. IEEE, 2020, pp. 1494–1498.
- [30] K. Pawar, Z. Chen, N. J. Shah, and G. F. Egan, "Suppressing motion artefacts in mri using an inception-resnet network with motion simulation augmentation," *NMR in Biomedicine*, vol. 35, no. 4, p. e4225, 2022, e4225 NBM-19-0154.R2.
- [31] D. Tamada, M.-L. Kromrey, H. Onishi, and U. Motosugi, "Method for motion artifact reduction using a convolutional neural network for dynamic contrast enhanced MRI of the liver," *arXiv e-prints*, p. arXiv:1807.06956, Jul. 2018.
- [32] M. W. Haskell, S. F. Cauley, B. Bilgic, J. Hossbach, D. N. Splitthoff, J. Pfeuffer, K. Setsompop, and L. L. Wald, "Network accelerated motion estimation and reduction (namer): Convolutional neural network guided retrospective motion correction using a separable motion model," *Magnetic Resonance in Medicine*, vol. 82, no. 4, pp. 1452–1461, 2019.
- [33] D. Ulyanov, A. Vedaldi, and V. Lempitsky, "Deep image prior," in *Proceedings of the IEEE conference on computer vision and pattern recognition*, 2018, pp. 9446–9454.
- [34] J. Lehtinen, J. Munkberg, J. Hasselgren, S. Laine, T. Karras, M. Aittala, and T. Aila, "Noise2Noise: Learning Image Restoration without Clean Data," *arXiv e-prints*, p. arXiv:1803.04189, Mar. 2018.
- [35] A. Krull, T.-O. Buchholz, and F. Jug, "Noise2void - learning denoising from single noisy images," in *2019 IEEE/CVF Conference on Computer Vision and Pattern Recognition (CVPR)*, 2019, pp. 2124–2132.
- [36] J. Chen, J. Chen, H. Chao, and M. Yang, "Image blind denoising with generative adversarial network based noise modeling," in *2018 IEEE/CVF Conference on Computer Vision and Pattern Recognition*, 2018, pp. 3155–3164.
- [37] E. M. Masutani, N. Bahrami, and A. Hsiao, "Deep learning single-frame and multiframe super-resolution for cardiac mri," *Radiology*, vol. 295, no. 3, pp. 552–561, 2020, pMID: 32286192.
- [38] Z. Wang, A. Bovik, H. Sheikh, and E. Simoncelli, "Image quality assessment: from error visibility to structural similarity," *IEEE Transactions on Image Processing*, vol. 13, no. 4, pp. 600–612, 2004.
- [39] X. Mao, Q. Li, H. Xie, R. Y. Lau, Z. Wang, and S. Paul Smolley, "Least squares generative adversarial networks," in *Proceedings of the IEEE international conference on computer vision*, 2017, pp. 2794–2802.
- [40] H. Li and J. Liu, "3D High-Quality Magnetic Resonance Image Restoration in Clinics Using Deep Learning," *arXiv e-prints*, p. arXiv:2111.14259, Nov. 2021.

- [41] J. Zbontar, F. Knoll, A. Sriram, T. Murrell, Z. Huang, M. J. Muckley, A. Defazio, R. Stern, P. Johnson, M. Bruno, M. Parente, K. J. Geras, J. Katsnelson, H. Chandarana, Z. Zhang, M. Drozdal, A. Romero, M. Rabbat, P. Vincent, N. Yakubova, J. Pinkerton, D. Wang, E. Owens, C. L. Zitnick, M. P. Recht, D. K. Sodickson, and Y. W. Lui, “fastMRI: An Open Dataset and Benchmarks for Accelerated MRI,” *arXiv e-prints*, p. arXiv:1811.08839, Nov. 2018.
- [42] F. Knoll, J. Zbontar, A. Sriram, M. J. Muckley, M. Bruno, A. Defazio, M. Parente, K. J. Geras, J. Katsnelson, H. Chandarana, Z. Zhang, M. Drozdal, A. Romero, M. Rabbat, P. Vincent, J. Pinkerton, D. Wang, N. Yakubova, E. Owens, C. L. Zitnick, M. P. Recht, D. K. Sodickson, and Y. W. Lui, “fastmri: A publicly available raw k-space and dicom dataset of knee images for accelerated mr image reconstruction using machine learning,” *Radiology: Artificial Intelligence*, vol. 2, no. 1, p. e190007, 2020, pMID: 32076662.
- [43] Y. Zhang, K. Li, K. Li, L. Wang, B. Zhong, and Y. Fu, “Image super-resolution using very deep residual channel attention networks,” in *Proceedings of the European conference on computer vision (ECCV)*, 2018, pp. 286–301.
- [44] Z. Lin, P. Garg, A. Banerjee, S. A. Magid, D. Sun, Y. Zhang, L. Van Gool, D. Wei, and H. Pfister, “Revisiting rcan: Improved training for image super-resolution,” *arXiv preprint arXiv:2201.11279*, 2022.
- [45] K. He, X. Zhang, S. Ren, and J. Sun, “Delving deep into rectifiers: Surpassing human-level performance on imagenet classification,” in *2015 IEEE International Conference on Computer Vision (ICCV)*, 2015, pp. 1026–1034.
- [46] S. Ioffe and C. Szegedy, “Batch normalization: Accelerating deep network training by reducing internal covariate shift,” in *International conference on machine learning*. PMLR, 2015, pp. 448–456.